Oxidation Stability of Multiwalled Carbon Nanotubes for Catalytic Applications

ARTICLE *in* CHEMISTRY OF MATERIALS · AUGUST 2010

Impact Factor: 8.35 · DOI: 10.1021/cm101234d

5 AUTHORS, INCLUDING:

Benjamin Frank
Unicat BASF Joint Lab (BasCat)
50 PUBLICATIONS **1,111** CITATIONS
SEE PROFILE

Dangsheng Su
Chinese Academy of Sciences
642 PUBLICATIONS **12,736** CITATIONS
SEE PROFILE

4462 *Chem. Mater.* **2010,** *22,* 4462–4470
DOI:10.1021/cm101234d

CHEMISTRY OF MATERIALS
Article

Oxidation Stability of Multiwalled Carbon Nanotubes for Catalytic Applications

Benjamin Frank, Ali Rinaldi, Raoul Blume, Robert Schlögl, and Dang Sheng Su*

Department of Inorganic Chemistry, Fritz Haber Institute of the Max Planck Society, Faradayweg 4-6, D-14195 Berlin, Germany

Received May 3, 2010. Revised Manuscript Received June 21, 2010

The oxidation of multiwalled carbon nanotubes (CNTs) was investigated with regard to a detailed prediction of the lifetime of this material as a catalyst for oxidative dehydrogenations. A power-law kinetics is found to be adequate for the description of CO_2 formation in the temperature range of 623−823 K and under O_2 partial pressures of 0.025−0.6 bar. The stability against oxidation can be enhanced by passivation with B_2O_3 or P_2O_5 and by high temperature treatment. The progress of oxidative degradation was monitored by TEM and Raman spectroscopy. A mechanistic study supported by high pressure XPS and SSITKA reveals full agreement with the established model of the oxidation of conventional carbon materials; however, the theory of sequential layer degradation as observed for single crystal graphite is not transferable to a technical grade CNT material, and instead, various modes of propagation of combustion sites are identified.

Introduction

The application of carbon nanotubes (CNTs) as catalysts for the oxidative dehydrogenation (ODH) of ethylbenzene[1−3] and especially of lower alkanes[4,5] is a novel strategy for a metal-free and sustainable alkene production.[6] The catalytic activity is determined by the presence of surface defects and oxygen functionalities which are regarded as "active sites" for ODH turnover.[5,7,8] As these sites are also a potential point of attack for oxygen species leading to carbon combustion,[9,10] a superior process design requires a well-optimized balance between alkene formation and CNT combustion. Unfortunately, the alkene yield in ODH reactions inevitably increases with temperature,[11] which is correlated to adsorption properties and the higher C−H bond strength in alkanes as compared to the corresponding alkenes.[12,13] The highly challenging approach is the selective generation of active sites, that is, basic ketonic and quinoidic groups,[7] combined with the removal of acidic functionalities, that is, anhydrides, being intermediates of carbon combustion and nonselective alkane conversion. A more pragmatic strategy is the selective blocking and stabilization of the carbon catalyst by combustion protectors such as boron or phosphorus oxide enabling the catalytic conversion at elevated temperatures.[4,5,14] In the present study, we investigate the effect of different methods for CNT stabilization by means of kinetic modeling for the prediction of the long-term suitability as a catalyst in the ODH of alkanes. In addition, mechanistic aspects of the carbon−oxygen reaction on CNTs are examined.

The investigation of CNT degradation at the absence of hydrocarbons in the feed gas represents the upper limit of reactivity. The oxidative chemical potential given by the effective oxygen partial pressure acting on the carbon surface under these conditions is the maximum and decreases at the presence of hydrocarbons in the feed, that is, ODH catalysis conditions. This is due to the "side" reactions as the catalytic hydrocarbon conversion, both selective and nonselective, and the condensation of hydrocarbons as soot or as part of a carbon self-repair mechanism at defect sites created during oxidation. Especially the aromatic hydrocarbons are known to act as antioxidants.[15] Thus, the CNT

*Corresponding author. Fax: +4930 84134405. Tel: +4930 84134464. E-mail: dangsheng@fhi-berlin.mpg.de.

(1) Zhang, J.; Su, D. S.; Zhang, A.; Wang, D.; Schlögl, R.; Hébert, C. *Angew. Chem., Int. Ed.* **2007**, *46*, 7319–7323.
(2) Su, D.; Maksimova, N.; Delgado, J.; Keller, N.; Mestl, G.; Ledoux, M.; Schlögl, R. *Catal. Today* **2005**, *102−103*, 110–114.
(3) Pereira, M. F. R.; Órfão, J. J. M.; Figueiredo, J. L. *Appl. Catal., A* **1999**, *184*, 153–160.
(4) Frank, B.; Zhang, J.; Blume, R.; Schlögl, R.; Su, D. S. *Angew. Chem., Int. Ed.* **2009**, *48*, 6913–6917.
(5) Zhang, J.; Liu, X.; Blume, R.; Zhang, A.; Schlögl, R.; Su, D. S. *Science* **2008**, *322*, 73–77.
(6) Su, D. S.; Zhang, J.; Frank, B.; Thomas, A.; Wang, X.; Paraknowitsch, J.; Schlögl, R. *ChemSusChem* **2010**, *3*, 169–180.
(7) Zhang, J.; Wang, X.; Su, Q.; Zhi, L.; Thomas, A.; Feng, X.; Su, D. S.; Schlögl, R.; Müllen, K. *J. Am. Chem. Soc.* **2009**, *131*, 11296–11297.
(8) Maciá-Agulló, J.; Cazorla-Amorós, D.; Linares-Solano, A.; Wild, U.; Su, D.; Schlögl, R. *Catal. Today* **2005**, *102−103*, 248–253.
(9) Bom, D.; Andrews, R.; Jacques, D.; Anthony, J.; Chen, B.; Meier, M. S.; Selegue, J. P. *Nano Lett.* **2002**, *2*, 615–619.
(10) Radovic, L. R. *J. Am. Chem. Soc.* **2009**, *131*, 17166–17175.
(11) Dinse, A.; Frank, B.; Hess, C.; Habel, D.; Schomäcker, R. *J. Mol. Catal. A: Chem.* **2008**, *289*, 28–37.
(12) Hodnett, B. K. In *Supported Catalysts and Their Applications*; Sherrington, D. C., Kybett, A. P., Eds.; Royal Society of Chemistry: 2001; pp 1−8.
(13) Zboray, M.; Bell, A. T.; Iglesia, E. *J. Phys. Chem. C* **2009**, *113*, 12380–12386.
(14) Sui, Z.; Zhou, J.; Dai, Y.; Yuan, W. *Catal. Today* **2005**, *106*, 90–94.
(15) Kobzova, R. I.; Oparina, E. M.; Tubyanskaya, G. S.; Levkina, N. K. *Chem. Technol. Fuels Oils* **1967**, *3*, 210–212.

Published on Web 07/14/2010

catalysts are expected to be much more stable under catalysis conditions than predicted from this study; however, the chosen concept is directed at the highest possible simplification of the experimental studies.

Numerous kinetic studies on the oxidation of various carbonaceous materials can be found in literature;[16−20] however, most of them make use of nonisothermal methods, that is, temperature programmed oxidation (TPO), for kinetic modeling. Here, the enormous exothermicity of carbon oxidation inevitably results in the thermal runaway in the high-temperature regime,[21] influencing the derived kinetic parameters by mass and heat transfer. Thus, for the prediction of low temperature oxidation rates, isothermal rate measurements are required.

The complex mechanism of carbon oxidation involves dissociative oxygen chemisorption, oxygen surface diffusion, and desorption of surface oxygen complexes.[10,21−24] There is a general agreement about the following steps (eqs 1−4),

$$2C + O_2(g) \rightarrow 2C(O) \quad (1)$$

$$C(O) \rightarrow CO(g) \quad (2)$$

$$C + C(O) + O_2(g) \rightarrow C(O) + CO_2(g) \quad (3)$$

$$2C(O) \rightarrow C + CO_2(g) \quad (4)$$

where C(O) stands for static and mobile oxygen surface species. A detailed and comprehensive mechanism of graphene combustion based on theory and a thorough review of literature has recently been proposed by Radovic.[10] According to this model both direct and indirect routes to CO_2 exist. Gas phase O_2 can either adsorb reversibly[4] on the basal graphene plane to form mobile epoxide-type oxygen or react directly with carbon edge atoms. The oxygen-saturated graphene edge is then highly susceptible to the mobile species resulting in rapid CO_2 formation. Reversely, it is also reported from theoretical studies that CO and CO_2 can heal defects in the graphite (0001) surface,[25] generating ketonic oxygen species, which is highly desirable for catalysis applications. Here, we focus on the reaction regime without substantial CO formation as here the carbon mass loss is so strong that a use of the carbon as a catalyst would no longer be relevant. In this way the present study is complementary to other works where the mass loss of carbon is the intended reaction.

Experimental Section

The raw material for this study is commercially available multiwalled CNTs (NC 3100, Nanocyl s.a.), functionalized and purified by HNO_3 treatment (denoted as oCNT) and further modified either with B_2O_3 (0.1, 1, and 5 wt %; 01B-, 1B-, and 5B-oCNT, respectively) or with P_2O_5 (5 wt %; 5P-oCNT). These have recently been introduced as selective catalysts in the ODH of propane.[4] Also, the heat treated CNTs, that is, annealed in inert Ar atmosphere at 1173/1973 K (oCNT-900/oCNT-1700, respectively), provide a useful catalytic performance[26] and have been investigated in this study. Furthermore, Baytubes (Bayer) and carbon nanofibers (PR24 LHT and HHT),[27] each HNO_3 washed, as well as activated carbon (Norit BRX) and highly ordered pyrolytic graphite (HOPG, Kropfmühl AF), were tested as reference samples. Nitric acid treatment was performed to remove the remaining metal/metal oxide (Fe, Co, Mn, Mg, Al) particles from the CNT/CNF syntheses (Figure S6, Supporting Information).

Oxidation rates have been determined in the temperature range of 623−823 K using O_2 fractions between 2.5−60% at ambient pressure (He balance) in a conventional quartz tubular reactor. To account for disordered carbon deposits on the nanocarbon surface[26] and for the initial process of surface functionalization, which can potentially cause misinterpretation of the oxidation rate measurements of graphitic materials, all the samples were preoxidized before the kinetic measurements. The structural and surface properties as a function of time-on-stream were studied by a long-term run, analyzing oCNT samples with different degrees of oxidation. Regarding the heat production, rate data were collected under reaction conditions, where the temperature increase over the catalyst bed length is calculated to be less than 5 K.

After the oxidation experiments, the samples were ex situ characterized by transmission electron microscopy (TEM, Philips CM 200 LaB6 at an acceleration electron voltage of 200 kV), Raman spectroscopy (ISA LabRam), N_2 physisorption at 77 K (Micromeritics 2375 BET), and thermogravimetric analysis (TGA, Netzsch STA 449C Jupiter equipped with HP DSC 827e, Mettler-Toledo, 5% O_2/Ar, 10 K min^{-1}). Oxygen surface species on the carbon surface of the freshly prepared samples as well as in situ during oxidation (after 24 h pretreatment in 5% O_2 at 673 K) were furthermore identified by X-ray photoelectron spectroscopy (XPS, ISISS beamline at BESSY II,[28] Berlin) for the oCNT and 1B-oCNT samples.

Results and Discussion

Kinetic Measurements. Below 773 K, the combustion of each carbon material predominantly yields CO_2, and rate data are described with high accuracy by an Arrhenius-type formal rate law (eq 5, Table 1, and Figure S1, Supporting Information).

$$\frac{dc(CO_2)}{dt} = k_0 \exp\left(\frac{-E_A}{RT}\right) p(O_2)^n \quad (5)$$

(16) Sørensen, L. H.; Gjernes, E.; Jessen, T.; Fjellerup, J. *Fuel* **1996**, *75*, 31–38.
(17) Córdoba, J.; Tamayo-Ariztondo, J.; Molina-Aldareguia, J.; Elizalde, M.; Odén, M. *Corros. Sci.* **2009**, *51*, 926–930.
(18) Li, C.; Brown, T. C. *Carbon* **2001**, *39*, 725–732.
(19) Brukh, R.; Mitra, S. *J. Mater. Chem.* **2007**, *17*, 619–623.
(20) Illeková, E.; Csomorová, K. *J. Therm. Anal. Calorim.* **2005**, *80*, 103–108.
(21) Stanmore, B. R.; Brilhac, J. F.; Gilot, P. *Carbon* **2001**, *39*, 2247–2268.
(22) Schlögl, R. *Chem. Unserer Zeit* **1994**, *28*, 166–179.
(23) Walker, P. L., Jr.; Taylor, R. L.; Ranish, J. M. *Carbon* **1991**, *29*, 411–421.
(24) Carlsson, J. M.; Hanke, F.; Linic, S.; Scheffler, M. *Phys. Rev. Lett.* **2009**, *102*, 166104.
(25) Xu, S. C.; Irle, S.; Musaev, D. G.; Lin, M. C. *J. Phys. Chem. C* **2009**, *113*, 18772–18777.
(26) Rinaldi, A.; Zhang, J.; Frank, B.; Su, D. S.; Abd Hamid, S. B.; Schlögl, R. *ChemSusChem* **2010**, *3*, 254–260.
(27) Tessonnier, J.; Rosenthal, D.; Hansen, T. W.; Hess, C.; Schuster, M. E.; Blume, R.; Girgsdies, F.; Pfänder, N.; Timpe, O.; Su, D. S.; Schlögl, R. *Carbon* **2009**, *47*, 1779–1798.
(28) Electron storage ring BESSY II. http://www.bessy.de (accessed January 18, 2010); new URL: http://www.helmholtz-berlin.de.

Table 1. Rate Parameters of Low-Temperature Oxidation and Structural Data of Investigated Carbon Samples

	E_A, kJ mol^{-1}	rate order $n(O_2)$	rate,[a] mmol g^{-1} h^{-1}	T_{50}, K	n_O, mmol g^{-1}	S_{BET}, m^2 g^{-1}	I_D/I_G
oCNT	138	0.52	0.27	671	0.166	541	3.48
01B-oCNT	143	0.52	0.53	665		497	2.37
5B-oCNT	144	0.47	0.099	705		357	3.89
5P-oCNT	167	0.47	0.044	756		358	4.49
oCNT[b]	127	0.48	2.1	614	0.183	556	4.31
oCNT-900[b]	127	0.54	0.32	659		675	3.51
oCNT-1700[b]	130	0.58	0.054	737		387	1.94
Baytubes	138	0.23	1.6	640	0.345	414	2.19
Norit BRX	117	0.69	1.0	648	0.810	1890	2.27
PR24 LHT	145	0.44	9.2×10^{-3}	753		36.3	1.65
PR24 HHT	146	0.49	0.019	773		56.5	0.80
HOPG	162	0.42	0.029	777	0.018	11.5	0.60

[a] 673 K, 10% O_2. [b] Neutralized by NaOH after nitric acid treatment.[26]

At higher temperatures, the formation of CO becomes relevant and can be described by a similar rate law. This, however, is neglected in the present study as described above, because here the degradation rate is too high for a potential catalytic use of the carbon material.

The data collected in Table 1 underline the enhanced resistance of oCNT against oxidation either by surface modification with high loadings of B_2O_3/P_2O_5 or by thermal treatment. The first method aims at the physical coverage of potential combustion sites,[29] whereas the latter one yields a highly ordered graphite surface with a low amount of surface inhomogeneities.[9] In both cases the reduced activation of gas phase oxygen is reflected in a higher activation energy. This is supported by the reference samples tested. Activated carbon provides the lowest activation energy and a poor stability, whereas both high temperature treated PR24 carbon nanofibers and the graphite samples are highly resistant against oxidation. The metal contents of all the samples collected in Table 1 determined by carbon combustion are below the detection limit of the applied TG analyzer ($<0.1\%$). The characteristic temperatures of 50% carbon combustion well correlate with the oxidation rates from quasi steady-state measurements. This is not the case for the BET surface areas, a phenomenon which is due to the anisotropic nature of graphitic materials leading to a topochemical control of the oxidation. The active surface area (ASA),[30,31] which mainly consists of graphene edge sites terminated by oxygen functional groups, is more representative for carbon reactivity, and a sufficient correlation with the oxygen concentration in selected carbon samples with the oxidation rate can be seen in Table 1.

The low stability of the Baytubes may refer to a higher amount of amorphous carbon and high concentration of defects as compared to the NC 3100 material[27] leading to rapid thermal runaway. The differences in oxidation stability of both differently prepared oCNT samples in Table 1 can presumably be ascribed to the presence of remaining Na. Remaining metal traces ($<0.1\%$) from the neutralization process strongly catalyze the carbon combustion,[32] indicated by a 10 kJ mol^{-1} lower activation energy. The pristine CNTs NC 3100 obtained by Nanocyl contain about 0.3 wt % metal oxide residues from the catalytic production process and also provide a much lower stability.[4]

The physicochemical meaning of the reaction rate order of oxygen has recently been discussed. In general, the rate order in the range of $0 < n < 1$ indicates a complex multistep surface reaction rather than a direct attack of O_2 at the carbon atom to be gasified, which would result in a first order rate law. A constant rate order over the wide range of experimental conditions can be assigned to the surface in homogeinity, whereas the rate order itself is suggested to increase with a decreasing degree of graphitization of the carbon specimen.[33] This agrees well with the activated carbon and the graphite samples but cannot be generalized from the data given in Table 1. Especially for the samples with similar morphology the tendency is inverse, for example, for the oCNT sample treated at different temperatures or for the two PR24 samples; hence, there must be other structural factors governing the rate order of O_2.

The validity of the kinetic parameters is confirmed by a long-term study of oCNT combustion. Figure 1a nicely reflects the very good agreement between experimental and predicted weight loss within up to almost 150 h time on stream, which corresponds to a weight loss of 50%. The deviation after the first cycle originates from the initial desorption of water from the fresh oCNTs (see arrow in Figure 1a). The experiment was frequently interrupted to take CNT samples of approximately 100 mg for structural characterization, that is, after 6.8, 25.9, 79.2, and 145.5 h. Except for the first hour time-on-stream the oxygen conversion was below 3% all the time (Figure 1b). This may refer to the initial combustion of carbonaceous material attached to the CNTs, which is highly functionalized by the HNO_3 treatment.[26] This is confirmed by a decrease of both the average CNT diameter and the intensity ratio of disordered (D) to graphitic (G) carbon bands I_D/I_G observed in the Raman spectra (Table 2). In addition, it was observed that in the initial period of each reaction sequence the oxygen conversion is slightly higher than in a pseudo-steady state (Figure 1b). The exposure of the carbon material to ambient

(29) McKee, D. W. *Chem. Phys. Carbon* **1991**, *23*, 174–232.
(30) Laine, N. R.; Vastola, F. J.; Walker, P. L. *J. Phys. Chem.* **1963**, *67*, 2030–2034.
(31) Vix-Guterl, C.; Couzi, M.; Dentzer, J.; Trinquecoste, M.; Delhaes, P. *J. Phys. Chem. B* **2004**, *108*, 19361–19367.
(32) McKee, D. W. *Fuel* **1983**, *62*, 170–175.
(33) Hurt, R. H.; Haynes, B. S. *Proc. Combust. Inst.* **2005**, *30*, 2161–2168.

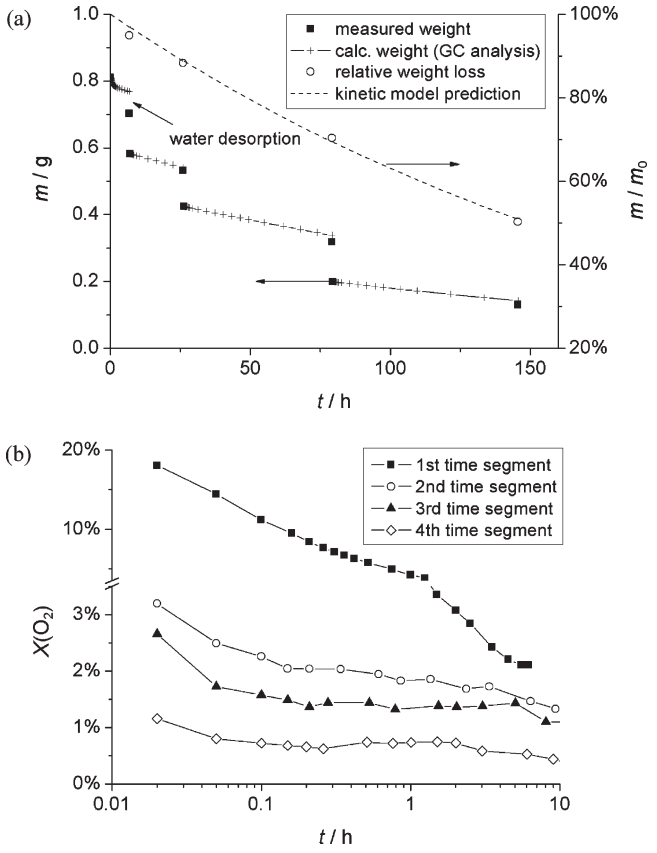

Figure 1. (a) Weight loss during the combustion of oCNTs; (b) initial oxygen conversion after exposure to ambient during oCNT sampling. 810 mg oCNT, 20% O_2 in He, 25 mL_n min^{-1}, 673 K.

Table 2. Structural Data of oCNT during Long-Term Combustion

	t_c, h	S_{BET}, m^2 g^{-1}	I_D/I_G	d, nm
pCNT	0	300	3.03	9.9
oCNT	0	541	3.48	9.2
oCNT	6.8	548	3.28	8.8
oCNT	25.9	563	3.24	8.6
oCNT	79.2	583	3.35	8.8
oCNT	145.5	590	3.59	10.3

at the sampling points leads to the adsorption of small amounts of water preferentially at the defect sites.[34,35] The hydrated surface species are apparently more susceptible to the reaction with O_2. The decrease of reaction rate is accompanied by the rapid discharge of water from the reactor with the reactant flow as monitored by GC analysis. It is an interesting analogy that water in trace amounts also catalyzes the oxidation of vanadia clusters.[36]

Structural Characterization. Details about the characterization of NC 3100 derived CNT samples can be found elsewhere.[4,26,27] Raman spectra (Figure 2) were deconvoluted following the procedure by Sadezky et al.[37] to estimate the degree of disorder in the carbon samples, that is, the intensity ratio of defective (structurally and

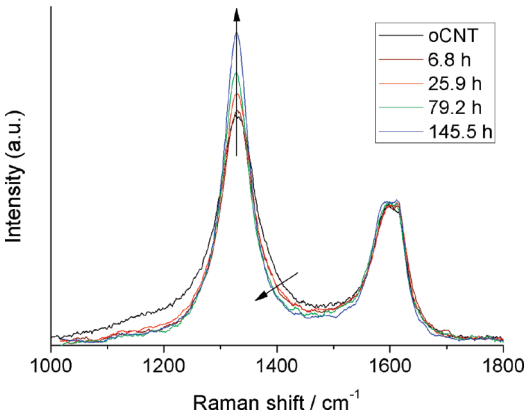

Figure 2. Raman spectra of oCNT after combustion for 6.8 h (a, b), 25.9 h (c, d), 79.2 h (e, f), and 145.5 h (g–j); intensity normalized at the G-band around 1600 cm^{-1}.

topologically as well as amorphous carbon) to ordered (graphitic) carbon atoms I_D/I_G. These values, together with the specific surface areas, are listed in Table 1. Further details and the fit exemplarily shown for oCNTs after 25.9 h of combustion can be found in the Supporting Information (Table S1, Figure S2). For the long-term study of oCNT combustion (Figure 1), these data are listed in Table 2 as a function of the combustion time t_c together with those of the pristine NC 3100 material (pCNT).

Surface areas and I_D/I_G values shown in Table 2 slightly increase with the progress of combustion indicating the formation of defects and holes in the CNTs. As compared to the TEM analysis, the Raman characterization shows a poorly sensitive response toward the microstructural changes in the combustion experiments performed in this study. This can be attributed to the much higher matrix element from the G peak signal compared to the D peak signal.[38] During the first 6.8 h time on stream a peak sharpening of the D band can be observed which indicates the initial cleaning of the CNT from amorphous carbon debris (Figure 2). After this process the peak width remains constant; however, the D band intensity increases relative to the G band, pointing at the continuous generation of defects and the stepwise degradation of the graphitic CNT structure during oxidation.

The structural transformation is well confirmed by TEM analysis. Figure 3 illustrates the structural damage inflicted on the CNTs as a result of combustion. The disordered structures are evidence of the partial gasification of oCNT by oxygen. The discontinuity of the graphene fringes in the TEM micrographs represents the most conspicuous indication of combustion in the CNTs. The formation of pits and wall thinning are frequently observed. It is reported that sites with topological defects such as the caps contain bond strain and thus are more reactive toward oxygen attack than smooth graphene walls along the CNT axis.[39] However, from the TEM micrographs it is evident that this cannot be generalized for this sample. After the first 6.8 h of combustion some CNTs still retain the close cap structure and some

(34) Zhanpeisov, N. U.; Zhidomirov, G. M.; Fukumura, H. *J. Phys. Chem. C* **2009**, *113*, 6118–6123.
(35) Allouche, A.; Ferro, Y. *Carbon* **2006**, *44*, 3320–3327.
(36) Frank, B.; Fortrie, R.; Hess, C.; Schlögl, R.; Schomäcker, R. *Appl. Catal., A* **2009**, *353*, 288–295.
(37) Sadezky, A.; Muckenhuber, H.; Grothe, H.; Niessner, R.; Pöschl, U. *Carbon* **2005**, *43*, 1731–1742.
(38) Robertson, J. In *Graphite and Precursors*; Delhaès, P., Ed.; Gordon and Breach Science Publishers: Amsterdam, 2001; p 249.
(39) Ajayan, P. M.; Ebbesen, T. W.; Ichihashi, T.; Iijima, S.; Tanigaki, K.; Hiura, H. *Nature* **1993**, *362*, 522–525.

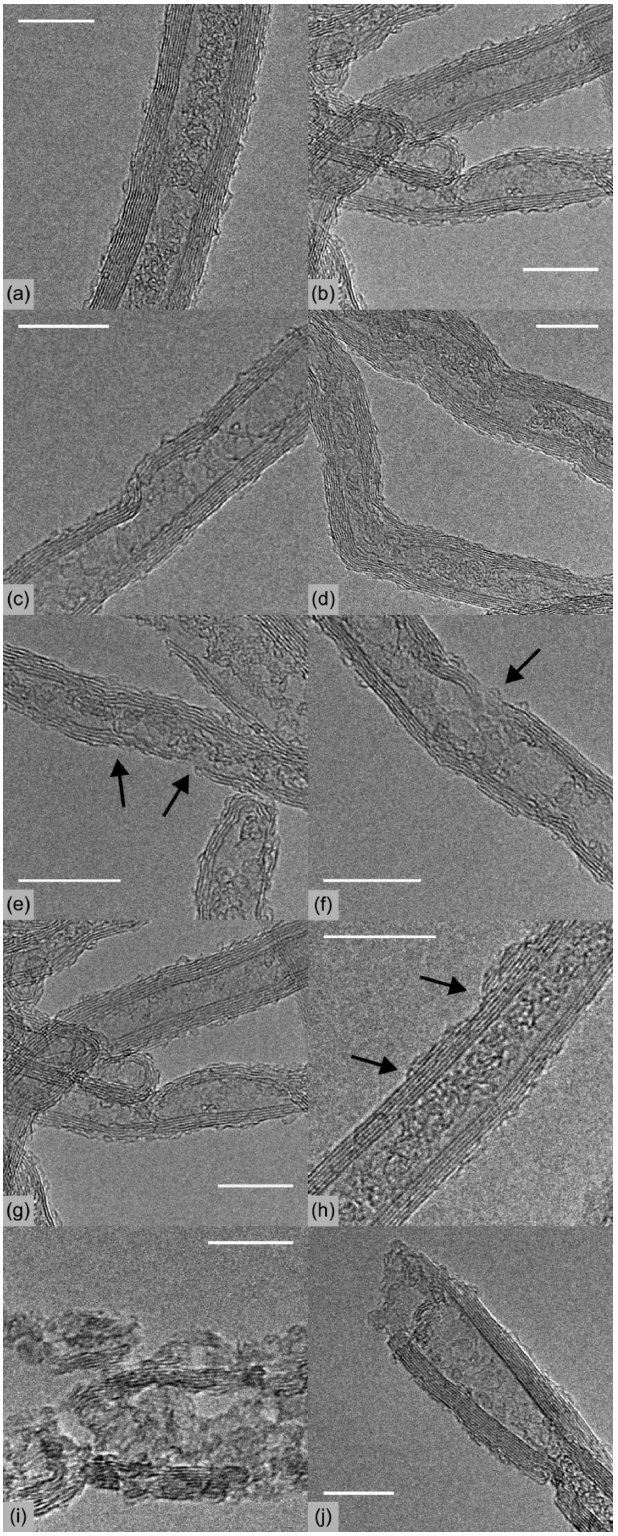

Figure 3. TEM images of oCNT after combustion for 6.8 h (a,b), 25.9 h (c,d), 79.2 h (e,f), and 145.5 h (g−j); scale bar 10 nm.

oxidation pits are located away from the topological defect site (Figure S3, Supporting Information). These observations point out that the initiation of the combustion is not limited to the strongly curved sites such as tips and bendings but is also located at the (defective) cylindrical regions of the CNTs.[40] Amorphous carbon debris and prismatic edges present at the CNT surface are more susceptible toward combustion than the basal plane of defect-free CNTs. Hence, these sites can initiate the combustion and create hotspots to propagate to the graphitic CNT surface.[41]

In addition the broad distribution of topological and structural defects in the CNTs with varying diameters are very likely to contribute to the various combustion patterns observed in oCNT samples. At least there are three distinct combustion propagation modes observed in the oCNT sample: (i) layer-by-layer mode resulting in thinner CNTs (Figure S4, Supporting Information), (ii) successive formation of pits in each graphene layer giving smaller holes in deeper layers (Figure S3d, Supporting Information), and (iii) formation of pits with uniform size in all layers (Figure 3j). Successive and simultaneous gasification of all layers in the CNTs reflects the various defects present in the sample that can initiate the combustion.[41]

The more rapid combustion was observed on the CNTs with smaller diameter. Especially after the first 6.8 h of combustion, pit holes and thinning are more frequently observed on thin CNTs. Consequently, after long-term combustion the diameter distribution increases due to preferential combustion of the thin CNTs (Figure S5, Supporting Information).[42] It is suggested that the strain caused by the high curvature of the graphene sheet in small diameter CNTs is a dominant factor to raise the reactivity for the initiation of oxidation.[43] The length distribution of the CNTs is difficult to evaluate due to their entangled texture. However, from the typical jagged open end features frequently observed in the samples, it is assumed that the combustion shortened and/or cut the CNTs.[44]

The reaction conditions for long-term combustion were adjusted to minimum oxygen conversion thus minimizing autocatalytic oxidation and thermal runaway. As the oCNT sample was treated with concentrated HNO_3, it is also noteworthy that the oxidative acid treatment can already cause damage to the CNT walls. The typical combustion features in the carbon microstructure become more obvious after the longer period of combustion. Here, pit holes of varying sizes are observed on the CNTs together with indications that oxidation debris is formed as the combustion progresses.[44] The TEM analysis does not allow to distinguish whether the amorphous structures attached to the CNTs surfaces originate from the highly oxidized graphene layers as oxidation debris or from remaining amorphous carbon. However, the presumption that amorphous carbon has a higher reactivity toward oxygen than the graphitic basal plane clearly points out that the amorphous carbon deposits are intermediates of CNT combustion.

(40) Pumera, M. *Chem. Asian. J.* **2009**, *4*, 250–253.
(41) Shimada, T.; Yanase, H.; Morishita, K.; Hayashi, J.; Chiba, T. *Carbon* **2004**, *42*, 1635–1639.
(42) Statistics is based on CNTs with intact tubular structure rather than open fragments.
(43) Yao, N.; Lordi, V.; Ma, S. X. C.; Dujardin, E.; Krishnan, A.; Treacy, M. M. J.; Ebbesen, T. W. *J. Mater. Res.* **1998**, *13*, 2432.
(44) Tran, M. Q.; Tridech, C.; Alfrey, A.; Bismarck, A.; Shaffer, M. S. *Carbon* **2007**, *45*, 2341–2350.

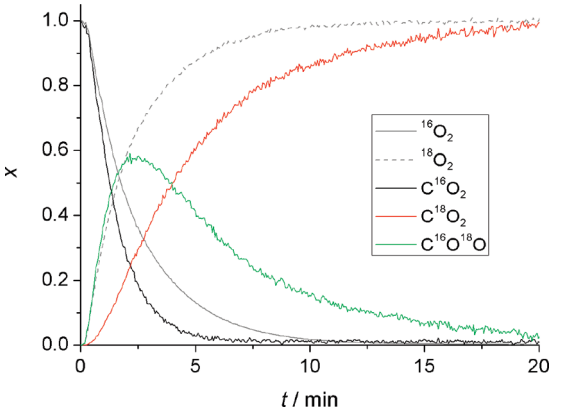

Figure 4. Transient responses of O_2 and CO_2 isotope signals to switching the feed from a 2% $^{16}O_2$/98% Ne to a 2% $^{18}O_2$/2% Ar/96% Ne gas mixture; 500 mg of oCNTs, 10 mL_n min^{-1}, 673 K.

At the sites where extensive combustion takes place, short remaining graphene stacks or unzipped graphene layers were also observed. A trace amount of remaining catalyst particles attached to the edges of CNTs was also observed by TEM, indicating their participation in catalytic combustion (Figure S6, Supporting Information). This contribution, however, is assumed to be negligible with regard to the overall oxidation rate.

Isotopic Tracer Experiments. The nature and impact of both the direct and indirect reaction pathways to CO_2 formation was investigated in detail by the steady state isotopic transient kinetic analysis (SSITKA). The samples differing most in the reaction order were subjected to a switch from $^{16}O_2$ to its isotopic tracer $^{18}O_2$ during oxidation. For oCNTs, the transient responses of $C^{16}O_2$, mixed labeled $C^{16}O^{18}O$, and doubly labeled $C^{18}O_2$ are shown in Figure 4.

In each case a huge amount of $C^{16}O^{18}O$ is formed as an intermediate product bringing up the predominant role of the dissociative oxygen activation for the degradation of each carbon material.[10,45,46] The long tailing of the $C^{16}O^{18}O$ response is in full agreement with the 0.5th reaction rate order of oxygen and the sequential multistep reaction mechanism described above. However, the higher the degree of graphitization of the sample, the lower the amount of mixed labeled $C^{16}O^{18}O$ detected. In particular, with regard to the statistically expected distribution of CO_2 isotopes[47] the total amount of $C^{16}O^{18}O$ formed is 121% for graphite, 178% for oCNTs, and 223% for activated carbon. Thus, in the low-temperature regime one can most likely exclude the direct attack of gas phase oxygen on surface functionalities or defects, which is the only pathway to yield doubly labeled $C^{18}O_2$ in excess to the amount statistically formed via the dissociative pathway. Instead, the observed tendency can probably be ascribed to the degree of surface functionalization, which increases in the order graphite < CNTs < activated carbon and serves as a reservoir for ^{16}O atoms to produce different amounts of mixed labeled CO_2. The SSITKA experiment with the P-oCNTs yields a lower amount of mixed labeled $C^{16}O^{18}O$ than for the oCNTs (148%, Supporting Information). In addition, the signal shows less pronounced tailing. As the TPD study of these catalysts after ethane ODH reveals an almost unchanged oxygen content of oCNT and P-oCNT samples,[48] this indicates that most of the surface oxygen species on P-oCNTs are completely passivated.

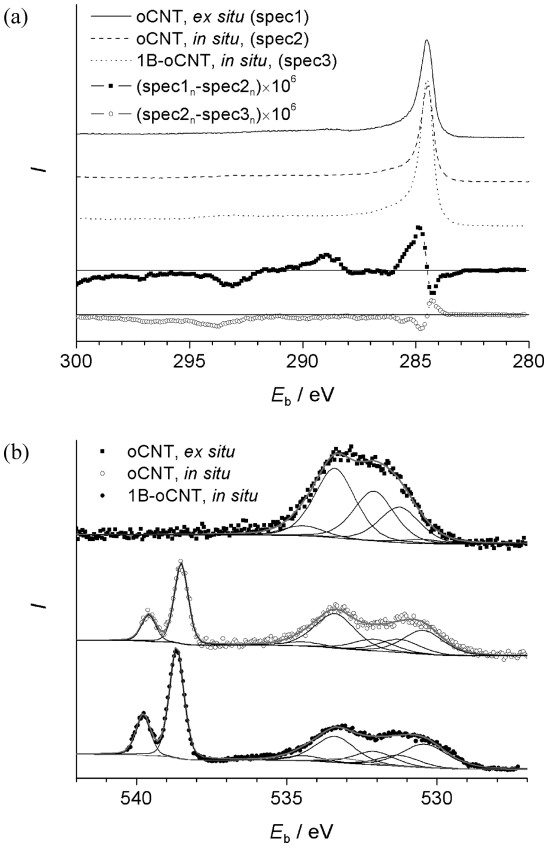

Figure 5. XPS spectra of the C 1s region (a) and of the O 1s region (b) of oCNT and 1B-oCNT. Ex situ conditions 298 K and UHV; in situ conditions 723 K and 0.5 mbar O_2.

Table 3. Peaks Used for O 1s XPS Spectra Fit

E_b, eV[a]	species
539.8, 538.7	O_2 (gas)
534.4	water
533.4	C−O in esters, anhydrides, and carboxylic groups
533.2	B_2O_3
532.1	hydroxyls, ethers, and C=O in esters and anhydrides
531.3	C=O in ketones
530.5	C=O in ketones

[a] Fitting tolerance ±0.05 eV.

Surface Analysis by XPS. XPS spectra of oCNT with and without B_2O_3 are presented in Figure 5a (C 1s region) and Figure 5b (O 1s region). Except for boron in 1B-oCNT (Figure S7, Supporting Information), no other elements

(45) Crick, T. M.; Silveston, P. L.; Miura, K.; Hashimoto, K. *Energy Fuels* **1993**, *7*, 1054–1061.
(46) Zhuang, Q.; Kyotani, T.; Tomita, A. *Energy Fuels* **1995**, *9*, 630–634.
(47) Considering the surface reaction to be sufficiently fast, the statistical composition of CO_2 isotopes follows the ratio of O_2 isotopes with binomial distribution: $x(C^{16}O_2) \propto x(^{16}O_2)^2$; $x(C^{18}O_2) \propto x(^{18}O_2)^2$; $x(C^{16}O^{18}O) \propto 2x(^{16}O_2)\,x(^{18}O_2)$.
(48) Frank, B.; Morassutto, M.; Schomäcker, R.; Schlögl, R.; Su, D. S. *ChemCatChem* **2010**, *2*, 644–648.

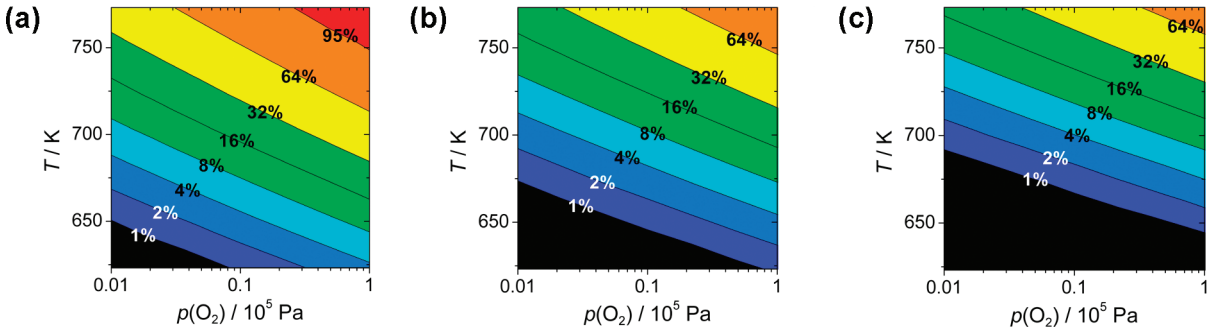

Figure 6. Fraction of differently treated CNTs combusted after 24 h time on stream in a O_2/He gas mixture: (a) oCNTs, (b) 5B-oCNTs, (c) 5P-oCNTs.

were detected in the surveys. The elemental compositions are given in the Supporting Information (Table S2). The C 1s spectra are dominated by the peak of graphitic carbon at 284.5 eV which has been used for calibration of the energy scale. This disregards the possibility that an energy shift may be chemically induced; however, it allows for the analysis of difference spectra, which reveal a sharpening at the high-energy side of this peak during oxidation. These indicate a higher degree of order being attained by selective removal of disordered material. In addition C−O functionalities found at 288−290 eV are almost completely removed. In contrast, in situ C 1s spectra of oCNT and 1B-oCNT are quite similar; the graphitic C peak appears to be slightly broader for the B_2O_3 modified sample which can be attributed to the protecting and stabilizing properties of this composite.

XPS spectra of the O 1s region have been deconvoluted (for details see Supporting Information), and at least seven oxygen species were included (Table 3). Their assignment is based on literature.[49−53]

The surface of HNO_3 treated oCNT is highly functionalized, and three oxygen species at around 533.4, 532.1, and 531.1 eV are dominant. Under reaction conditions the oxygen surface concentration decreases by approximately 25% in agreement with the disappearance of the 288−290 eV band in the C 1s spectrum. The nucleophilic species at the low energy side almost disappear, and a new species is formed at around 530.5 eV indicating a change in the local environment of ketonic or quinoidic terminations. Again, the in situ spectra of oCNT and 1B-oCNT look quite similar. The loss of ketone-, hydroxyl-, and ether-like oxygen indicates that these species are reactive toward oxygen as they would not thermally decompose at the temperature as low as 673 K.[4,49] However, these are not the intermediates of CNT combustion. On the other hand, from the typical TPD pattern of HNO_3 treated nanocarbons it is obvious that the loss of surface oxygen is mainly due to the decomposition of carboxylic acid and anhydride at up to 673 K.[4,49] Under reaction conditions these species are still observable in relevant quantities and thus must be regenerated during the CNT combustion process, which appears to be independent from the B_2O_3 loading. The species generated at around 530.5 eV is scarcely reported in literature. Residual metal oxide, however, can be excluded from the survey spectra giving no indication of, for example, Fe, Co, or Ni, neither under ex situ nor under in situ conditions. Some authors suggest a ketonic or quinoidic oxygen species.[50,54] However, it must be considered that most of the assignments in literature are based on ex situ studies, where such species might be not visible. Furthermore, one has to consider that different CNTs treated the same way, for example, by HNO_3, can lead to different grades of functionalization.[55]

Discussion

The kinetic data can be used to predict the lower limit of the lifetime of carbon catalysts under oxygen containing gas atmosphere, that is, in ODH reactions. Figure 6(a−c) displays the loss fraction of CNTs after 24 h time on stream as a function of temperature and O_2 concentration. The unmodified oCNT sample (Figure 6a) apparently cannot be used for ODH catalysis in the viewpoint of long-term stability, as a weight loss of < 1 wt % per day is only observed for temperatures below 650 K and O_2 partial pressures < 10 kPa. From Table 1 it is evident that the effect of 0.1 wt % B_2O_3 appears to be counterproductive for catalyst protection, even though it is remarkable for catalytic performance.[4] Indeed, small amounts of boron were found to catalyze the carbon combustion.[56] A certain range for process design with reasonable catalyst lifetimes does not open below 5 wt % B_2O_3 (Figure 6b). Here, the reaction conditions can be varied between 623−673 K and 1−10 kPa O_2 without substantial catalyst loss during the reaction. This is confirmed by ODH long-term experiments, showing no deactivation for the period of up to 200 h.[4] The most effective catalyst protection, however, is achieved by CNT modification with P_2O_5 (Figure 6c).

(49) Figueiredo, J. L.; Pereira, M. F. R. *Catal. Today* **2010**, *150*, 2–7.
(50) Schlögl, R.; Loose, G.; Wesemann, M. *Solid State Ionics* **1990**, *43*, 183–192.
(51) NIST X-ray Photoelectron Spectroscopy Database. http://srdata.nist.gov/xps (accessed January 4, 2010).
(52) Arrigo, R. Nitrogen Functionalization of CNFs and Application in Heterogeneous Catalysis. Ph.D. thesis, Berlin, 2009.
(53) Siegbahn, K. *ESCA applied to free molecules*; North Holland Publishing: Amsterdam, 1969.
(54) Walczyk, M.; Świątkowski, A.; Pakuła, M.; Biniak, S. *J. Appl. Electrochem.* **2005**, *35*, 123–130.
(55) Pumera, M.; Šmíd, B.; Veltruská, K. *J. Nanosci. Nanotechnol.* **2009**, *9*, 2671–2676.
(56) Radovic, L. R.; Karra, M.; Skokova, K.; Thrower, P. A. *Carbon* **1998**, *36*, 1841–1854.

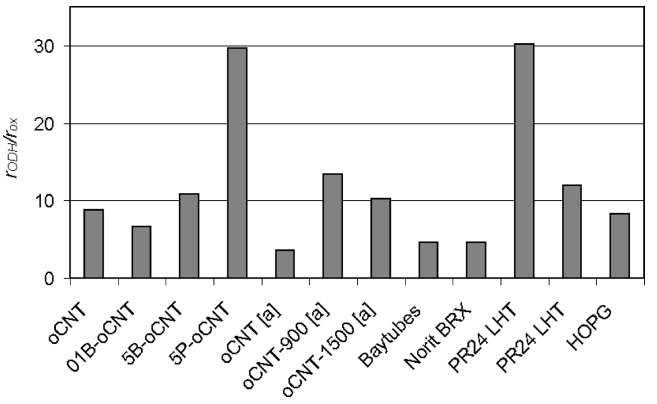

Figure 7. Correlation of the activity of some carbon catalysts in the ODH of propane with their stability against oxidation. The reaction conditions for ODH are $C_3H_8/O_2/He = 1:1:8$ and for the oxidation O_2:He = 1:9 at 673 K, respectively; [a]: samples neutralized with NaOH after HNO_3 treatment.

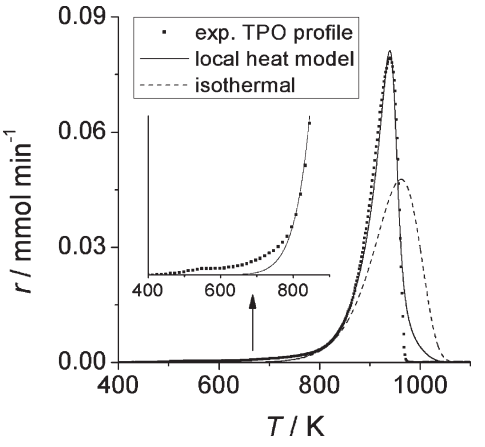

Figure 8. TPO profile of oCNTs, 5 K min^{-1}, 5% O_2 in He.

If correlated to catalytic turnover in the ODH of propane (Figure 7), the oxidation rate gives a relative estimate about the effective catalyst protection by means of a quasi turnover number (qTON). Here, the modification with P_2O_5 appears to be most effective giving a qTON of up to 30, which is close to the PR24 and the graphite samples. The lowest qTONs (3−5) are provided by the nonannealed oCNTs containing trace amounts of sodium, by the Baytubes, and by activated carbon. It should be mentioned that the qTONs and the true turnover numbers of carbon atoms (average number of ODH cycles per carbon atom before combustion) can differ strongly, as indicated by ODH long-term studies.[4,5] A competitive mechanism by substrate or oxygenate adsorption and even the regeneration of active sites by carbon atoms supplied by the hydrocarbon or CO_x[25] is the subject of current research. Indeed, for relatively heavy ODH substrates such as ethylbenzene, which tend to form coke deposits even at low reaction temperatures,[1] a catalyst weight increase is observed at low O/C ratios.[57]

Furthermore, the kinetic data can be used to accurately model TPO profiles (Figure 8). However, given the kinetic data from Table 1, the experimental TPO profile cannot be reflected sufficiently without correction for temperature gradients at higher temperatures/oxidation rates, which induces both the sharper curve shape and a shift of the TPO maximum to lower temperatures. This illustration strongly suggests to use TPO data for kinetic analysis not until isothermicity has been explicitely proven. Thanks to the aging period before kinetic measurements, the combustion/decomposition of volatile carbon species observed by TPO (Figure 8, inset) does not falsify the model curve for bulk oxidation (> 800 K).

The mechanistic investigations of CNT combustion are in agreement with previous studies over conventional carbon materials.[10,22] The rate order of oxygen in the range $0 > n > 1$ and isotopic tracer studies reveals that, at least for the CO_2 formation below 673 K, oxygen dissociates on an active site which is most likely the (0001) basal plane. Radovic proposed epoxide-type intermediate structures for this reaction step.[10] This process is not completely irreversible[4] and provides a reservoir of reactive and mobile oxygen species; however, the basal plane is highly resistant against gasification. The CO_2 formation occurs at the active surface area (ASA) terminating the basal planes, which represent a negligible fraction of the total surface area (TSA). Thus the direct O_2 adsorption can be neglected. These sites are defects and functional groups at the edges of the basal plane.[10] XPS analysis shows that carboxylic acid and anhydride are the most abundant surface intermediates among the oxygen functional groups, whereas other species such as ether, hydroxyl, or ketonic groups are less stable and will be replaced first during edge oxidation of the graphene layer. An increased reactivity after air (humidity) exposure indicates that the carboxylic acid is more reactive in the reaction with oxygen than the carboxylic anhydride functionality. The stepwise combustion of graphene layers as observed for ideal graphite crystals[50,58] is not observed in such perfection for the multiwalled CNTs. Even though some indications such as the formation of single- and multisteps or wall thinning could be confirmed by TEM analysis, the defective structure of the applied technical grade material brings up nonideal combustion behavior. It could be observed that hot spots are created far away from the theoretical basal plane edge, which is the CNT tip. From these points the oxidation is not limited to two-dimensional expansion but also penetrates the CNT wall in the radial direction. One explanation might be the reaction heat of oxidation of the outermost graphene layer containing a defect. This can possibly raise the local temperature to increase the reactivity of the next (intact) graphene layer to a critical level. Furthermore, during oxidation a certain amount of amorphous carbon or unfolded graphene sheets is frequently observed. These presumably highly reactive carbon structures are ubiquituous intermediates of CNTs combustion.

(57) Alkhazov, T. G.; Lisovskii, A. E.; Gulakhmedova, T. K. *React. Kinet. Catal. Lett.* **1979**, *12*, 189–193.

(58) Hughes, E. E. G.; Thomas, J. M. *Nature* **1962**, *193*, 838–840.

Acknowledgment. The authors greatly appreciate financial support by the EnerChem project of the Max Planck Society (URL: http://www.enerchem.de) and by the Federal Ministry of Education and Research (BMBF) in the frame of the InnoCNT alliance (URL: http://www.inno-cnt.de), subproject Carboscale.

Supporting Information Available: Parity plot of kinetic fits, details of Raman spectra fits, additional TEM micrographs, diameter distributions of CNTs, and XPS spectra of B 1s region (PDF). This material is available free of charge via the Internet at http://pubs.acs.org.